



Kent Academic Repository

Pickup, David M., Moss, Rob M., Qui, D., Newport, Robert J., Valappil, Sabeel P., Knowles, Jonathan C. and Smith, Mark E. (2009) *Structural characterization by x-ray methods of novel antimicrobial gallium-doped phosphate-based glasses*. *Journal of Chemical Physics*, 130 (6). 064708. ISSN 0021-9606.

Downloaded from

<https://kar.kent.ac.uk/19150/> The University of Kent's Academic Repository KAR

The version of record is available from

<https://doi.org/10.1063/1.3076057>

This document version

Author's Accepted Manuscript

DOI for this version

Licence for this version

UNSPECIFIED

Additional information

Grant Number from STFC EP/C000714 EP/C000633 GR/T21080

Versions of research works

Versions of Record

If this version is the version of record, it is the same as the published version available on the publisher's web site. Cite as the published version.

Author Accepted Manuscripts

If this document is identified as the Author Accepted Manuscript it is the version after peer review but before type setting, copy editing or publisher branding. Cite as Surname, Initial. (Year) 'Title of article'. To be published in *Title of Journal*, Volume and issue numbers [peer-reviewed accepted version]. Available at: DOI or URL (Accessed: date).

Enquiries

If you have questions about this document contact ResearchSupport@kent.ac.uk. Please include the URL of the record in KAR. If you believe that your, or a third party's rights have been compromised through this document please see our [Take Down policy](https://www.kent.ac.uk/guides/kar-the-kent-academic-repository#policies) (available from <https://www.kent.ac.uk/guides/kar-the-kent-academic-repository#policies>).

Structural Characterisation by X-ray Methods of Novel Antimicrobial Gallium-Doped Phosphate-Based Glasses

D. M. Pickup, R. M. Moss, D. Qiu, R. J. Newport
School of Physical Sciences, University of Kent, Canterbury CT2 7NH, UK

S. P. Valappil, J. C. Knowles
Division of Biomaterials and Tissue Engineering, UCL Eastman Dental Institute, London WC1X 8DL, UK

M. E. Smith
Department of Physics, University of Warwick, Coventry CV4 7AL, UK

Antimicrobial gallium-doped phosphate-based glasses of general composition $(\text{P}_2\text{O}_5)_{0.45}(\text{CaO})_{0.16}(\text{Na}_2\text{O})_{0.39-x}(\text{Ga}_2\text{O}_3)_x$ (where $x = 0, 0.01, 0.03$ and 0.05) have been studied using the advanced synchrotron-based techniques of Ga K-edge X-ray absorption spectroscopy (XAS) and high-energy X-ray diffraction (HEXRD) to provide a structural insight into their unique properties. The results show that the Ga^{3+} ions are octahedrally coordinated. Furthermore, substitution of Na_2O by Ga_2O_3 strengthens the phosphate network structure because the presence of GaO_6 octahedra inhibits the migration of the remaining Na^+ ions. The results are discussed in terms of the use of Na_2O - CaO - P_2O_5 glasses as controlled-delivery devices for antimicrobial Ga^{3+} ions in biomedical applications. We are thereby able to relate the atomic-scale environment of the Ga^{3+} ions beneficially to the glass dissolution, and thus to their ability to disrupt bacterial cell activity by usurping the role of iron.

I. INTRODUCTION

The incidence of biomaterial-centred infection, often leading to revision surgery, underlies the need to improve the properties of existing biomaterials by combining them with effective antimicrobial agents¹. The causative organism in such infections is usually present as a biofilm², a complex aggregation of microbes marked by the excretion of a protective and adhesive matrix. At present, prophylaxis, often in the form of systemically administered antibiotics, is the main weapon against bacterial infection following implant surgery¹. The success of this method is limited, however, by the fact that the bacteria in biofilms are often resistant to antimicrobial agents and by the emergence of multi-resistant nosocomial pathogens such as MRSA and *Clostridium difficile*. Despite the recent increase in the number of reported MRSA and *Clostridium difficile* cases, only one new antibacterial drug with a novel mechanism of action has been introduced in the past three decades (linezolid), and very few new antibiotics are in the advanced stages of development³.

Recently, it has been demonstrated that gallium ions disrupt the iron metabolism of *Pseudomonas aeruginosa*, and exhibit antimicrobial and antibiofilm activity⁴. Due to the chemical similarity of Ga³⁺ with Fe³⁺ in terms of electric charge, ionic radius, electronic configuration and coordination number, gallium can substitute for iron in many biological systems. Since Ga³⁺ can not be reduced under the same conditions as Fe³⁺ and sequential redox reactions are critical for many of the biological functions of Fe³⁺, these functions are inhibited by gallium substitution⁵. This “Trojan horse” strategy can be exploited to disrupt iron metabolism in a wide range of bacteria. As well as *P. aeruginosa*, gallium has been shown to be effective

against the organisms causing tuberculosis⁶ and malaria⁷ in human beings, and in the treatment of *Rhodococcus equi* caused pneumonia in foals⁸.

The use of gallium ions as an antimicrobial agent could be significantly improved by the development of an effective means of delivery. Durable materials that can slowly release ions over long periods would be advantageous in such biomedical applications. Phosphate-based glasses (PBGs) containing calcium and sodium ions are both bioresorbable and biocompatible, and can act as a unique system for the controlled delivery of metal ions with the rate of release defined by the overall degradation rate of the glass⁹. Copper and silver ions have been incorporated into PBGs, and the glasses incorporated into wound dressings to prevent infection¹⁰ and also to control urinary tract infections in patients needing long-term indwelling catheters^{10,11}. In the present work, we are exploring the potential for combining the antibacterial activity of Ga³⁺ ions with a PBG controlled delivery system.

To this end we have recently developed novel quaternary gallium-doped PBGs (1, 3, 5 mol% Ga₂O₃) that have been characterised for their antimicrobial properties, physio-thermal properties, solubility and ion release. The results confirmed that the net bactericidal effect was due to Ga³⁺ ions, and a concentration as low as 1 mol % Ga₂O₃ was sufficient to mount a potent antibacterial effect. The dearth of new antibiotics in development makes gallium a potentially promising new therapeutic agent for pathogenic bacteria including *MRSA* and *C. difficile*¹². Moreover, gallium can inhibit bone resorption and stimulate bone formation¹³ and hence these novel glasses may also have applications in bone tissue engineering.

Key to a full understanding of these materials is knowledge of their atomic-scale structure. The network connectivity largely controls the overall dissolution of the glass, but this will be affected to some extent by the presence of gallium. The

extent of this effect will depend upon the structural environment of the Ga^{3+} ions and the nature of their bonding interaction with the network. Hence the aim of this study is to probe the structure of the novel gallium-doped PBGs using advanced synchrotron-based techniques: high-energy X-ray diffraction (HEXRD) to provide information on the overall network structure and Ga K-edge X-ray absorption spectroscopy (XAS) to study the environment of the Ga^{3+} ions.

II. EXPERIMENTAL

A. Glass preparation

Phosphate-based glasses were produced using NaH_2PO_4 (BDH, 98%), P_2O_5 (BDH, 98.5%), CaCO_3 (BDH, 97%) and Ga_2O_3 (Aldrich, 99.99%) as starting materials. The required amounts of each reagent were weighed into a Pt/10%Rh crucible (Johnson Matthey). The crucible was placed in a furnace preheated to 1100°C and left for 1 hour. The molten glass was then poured into a graphite mould preheated to 350°C and allowed to cool to room temperature. Four samples were prepared of general composition $(\text{P}_2\text{O}_5)_{0.45}(\text{CaO})_{0.16}(\text{Na}_2\text{O})_{0.39-x}(\text{Ga}_2\text{O}_3)_x$ (where $x = 0, 0.01, 0.03$ and 0.05).

B. High-energy X-ray diffraction

HEXRD data were collected on Station 9.1 at the Synchrotron Radiation Source (SRS), Daresbury Laboratory, UK. The finely powdered samples were enclosed inside a 0.5 mm thick circular metal annulus by kapton windows and

mounted onto a flat-plate instrumental set-up. The wavelength was set at $\lambda = 0.4858$ Å and calibrated using the K-edge of a Ag foil; this value was low enough to provide data to a high value of momentum transfer ($Q_{\max} = 4\pi\sin\theta/\lambda \sim 23$ Å⁻¹). The data were reduced using a suite of programs written in-house: the initial stage of analysis of XRD data from an amorphous material involves the removal of background scattering, normalization, correction for absorption and subtraction of the self-scattering term¹⁴. The resultant scattered intensity, $i(Q)$, can reveal structural information by Fourier transformation to obtain the pair-distribution function:

$$T(r) = T^0(r) + \int_0^{\infty} Qi(Q)M(Q)\sin(Qr) d(Q) \quad (1)$$

where $T^0(r) = 2\pi^2r\rho_o$ (r is the atomic separation between atoms and ρ_o is the macroscopic number density) and $M(Q)$ is a window function necessitated by the finite maximum experimentally attainable value of Q .

Structural information can be obtained from the diffraction data by modelling the Q -space data and converting the results to r -space by Fourier transformation to allow comparison with the experimentally determined pair-distribution function¹⁵. The structural parameters used to generate the Q -space simulation are varied to optimize the fit to the experimental data. The Q -space simulation is generated using the following equation:

$$p(Q)_{ij} = \frac{N_{ij}w_{ij}}{c_j} \frac{\sin QR_{ij}}{QR_{ij}} \exp\left[\frac{-Q^2\sigma_{ij}^2}{2}\right] \quad (2)$$

where $p(Q)_{ij}$ is the pair function in reciprocal space, N_{ij} , R_{ij} and σ_{ij} are the coordination number, atomic separation and disorder parameter, respectively, of atom i with respect to j , c_j is the concentration of atom j and w_{ij} is the weighting factor. The weighting factors are given by:

$$w_{ij} = \frac{2c_i c_j f(Q)_i f(Q)_j}{f(Q)^2} \quad \text{if } i \neq j \quad (3)$$

or,

$$w_{ij} = \frac{c_i^2 f(Q)_i^2}{f(Q)^2} \quad \text{if } i = j \quad (4)$$

where $f(Q)$ represents the Q -dependant X-ray form factors.

The errors associated with the HEXRD data arise mainly from the fitting process due to the problem of overlapping correlation shells. They have been estimated on the basis of the tolerance that a particular parameter may have without significantly changing the overall quality-of-fit. Some additional systematic error may occur from the data reduction process as a result of the approximations subsumed into the various data corrections (*e.g.* for Compton scattering), but past analysis of test-sample data, and data collected at different wavelengths, suggest that these errors are small compared to those arising from the numerical modelling of the experimental data.

C. X-ray Absorption Spectroscopy

Ga K-edge XAS measurements were made at room temperature on Station 16.5 at the SRS, Daresbury Laboratory, UK, with a ring energy of 2 GeV and a stored

current of 150-250 mA. The spectra were recorded in transmission mode using a double crystal Si(220) monochromator ($d = 1.92 \text{ \AA}$) and ionisation chambers to detect the incident and transmitted beam intensities. Finely-ground samples were diluted in polyethylene (Aldrich, spectrophotometric grade) and pressed into pellets to give a satisfactory edge jump and absorption. An encapsulated gallium foil and a third ionisation chamber were placed after the sample to allow an absorption spectrum of the foil to be collected simultaneously for the purpose of calibration of the energy scale. The energy scale was defined by assigning the point of maximum gradient on the absorption edge from the Ga foil to 10367 eV.

XANES spectra were collected from 50 eV below to 130 eV above the Ga K-edge in order to allow accurate background subtraction. A fine energy step of 0.4 eV was used around the edge. The data processing comprised conversion of the data to absorption versus energy, calibration of the energy scale, removal of the pre-edge background by straight-line fitting and removal of the post-edge background by fitting with a second-order polynomial. All the spectra were normalised to have an edge-step of 1. Each spectrum consisted of the sum of two scans. As well as the data from the gallium-doped PBGs, spectra were also collected from a series of crystalline reference materials containing Ga^{3+} ions in well-defined coordination geometries: quartz α - GaPO_4 , β - Ga_2O_3 and $\text{Ga}(\text{acac})_3$. The $\text{Ga}(\text{acac})_3$ was purchased commercially (Aldrich, 99.99%), whilst the quartz α - GaPO_4 and β - Ga_2O_3 were synthesized. The quartz α - GaPO_4 was prepared by precipitation from an aqueous mixture of GaCl_3 (Aldrich, 99.99%) and H_3PO_4 by the addition of NH_4OH . The product was separated by filtration, washed and dried before heating to 800 °C to remove ammonium and hydroxyl groups¹⁶. The β - Ga_2O_3 was prepared by calcination of Aldrich 99.99% Ga_2O_3 overnight at 1000 °C¹⁷. The gallium foil used for the calibration of the energy

scale was prepared by hot-pressing Aldrich 99.99% Ga metal between two sheets of filter paper and laminating the resulting construct in plastic.

Data were also collected in the EXAFS region for selected samples. The EXAFS spectra were collected over the range $k = 3 - 18 \text{ \AA}^{-1}$ with a step of 0.04 \AA^{-1} and a counting time of 1 to 10 s per point varying as k^3 ($k = \sqrt{2m_e/\hbar^2(E - E_0)}$, where m_e = mass is the rest mass of the electron, E = energy and E_0 = energy of the absorption edge). The programs EXCALIB, EXSPLINE and EXCURV98¹⁸ were used to extract the EXAFS signal and analyse the data. Least squares refinements of the structural parameters of our samples were carried out against the k^3 -weighted EXAFS signal to minimize the fit index, FI,

$$\text{FI} = \sum_i (k^3(\chi_i^{\text{T}} - \chi_i^{\text{E}}))^2 \quad (5)$$

where χ_i^{T} and χ_i^{E} are the theoretical and experimental EXAFS, respectively. The results of the refinements are reported in terms of the discrepancy index, R_{di} .

$$R_{\text{di}} = \frac{\int |(\chi^{\text{T}}(k) - \chi^{\text{E}}(k))| k^3 dk}{\int |\chi^{\text{E}}(k)| k^3 dk} \times 100\% \quad (6)$$

Quartz α -GaPO₄ was run as reference material to check the validity of our data analysis and also to allow refinement of the parameter *AFAC* (defined as the proportion of the photo-electrons taking part in an ‘EXAFS-type’ scattering event).

III. RESULTS

A. High-energy X-ray diffraction

Fig. 1 shows the HEXRD data from the PBGs containing 0 and 5 mol% Ga_2O_3 . HEXRD data from an amorphous material can give information on the atomic distances and occupancies within its structure. Such information is contained in the pair-distribution functions (PDFs) which are obtained by Fourier transformation of the corrected scattering data. The pair-distribution functions shown in Fig. 1 (b) were obtained by Fourier transformation of the curves in Fig. 1 (a). They exhibit four features that are characteristic of the structure of a PBG: an intense peak at 1.55 Å due to P–O bonding, a peak at 2.45 Å attributed mainly to the O···O nearest-neighbour distance, a shoulder on the low- r side of this peak due to Ca–O and Na–O bonding, and a peak at 2.95 Å assigned to the P···P distance¹⁹.

In order to identify the atomic correlations associated with gallium, we take a difference between the PDF from the glass containing no Ga_2O_3 and that containing 5 mol% Ga_2O_3 . The resulting difference PDF is shown in Fig. 2. This method does not completely isolate the correlations associated with gallium, even assuming that the two samples are structurally equivalent except for the substitution of Na_2O by Ga_2O_3 , because the X-ray weighting factors (*i.e.* a measure of the strength with which a given correlation scatters X-rays) for all the pair-wise correlations change as a function of glass composition; as a consequence, the other atomic correlations (mainly P–O, Na–O, Ca–O, O···O and P···P) do not completely cancel out. However, this difference method may reasonably be applied here because the compositions of the glass studied are such that the residual peaks due to the P–O, Na–O, Ca–O, O···O and P···P

correlations are small compared to those involving the gallium ions. This is illustrated by Fig. 3 which shows the X-ray weighting factors for the difference PDF, obtained by calculating the approximate weighting factors for each correlation at the two compositions and subtracting. The weighting factors used are approximate because they were calculated using the atomic number for each element rather than its X-ray form factor (*i.e.* using $F_{ij} = 2c_i c_j Z_i Z_j$ and $F_{ii} = c_i^2 Z_i^2$, where F_{ij} is the weighting factor for the i - j correlation, and c_i and Z_i are the concentration and atomic number of element i , respectively)²⁰. Examining Fig. 3, it can be seen that the Ga–O and Ga···P correlations are expected to contribute the most to the difference PDF. Indeed, the difference PDF does exhibit two intense peaks at 1.93 and 3.19 Å, respectively assigned, on the basis of the difference weighting factors, to Ga–O and Ga···P distances. Although no further quantitative information may be derived from the difference PDF, for the reason described above, the determination of the Ga–O and Ga···P distances is nonetheless valuable to the overall characterisation of the glass structure, and vital for the modelling of the HEXRD data.

Structural parameters (*i.e.* atomic distances, coordination numbers and the degree of disorder within a particular atomic correlation) can be obtained from HEXRD data by modelling the pair-distribution function. Using the peak assignments described above, we have simulated the PDFs shown in Fig. 1; the resultant structural parameters are given in Table I.

B. X-ray absorption spectroscopy

Extended X-ray absorption fine structure, EXAFS, spectroscopy provides information on the local structure around a given probe element by simulating the

experimental data using routines based upon curved-wave theory²¹. Here we collected Ga K-edge data from the glass samples containing 3 and 5 mol% Ga₂O₃; the structural parameters obtained from the simulation of the data are given in Table II. Two atomic correlations were observed, one at 1.93 Å due to a Ga–O distance and one at 3.18 Å ascribed to a Ga···P distance. These distances show excellent agreement with those determined from the HEXRD data. The structural parameters from the longer Ga···P correlation should be treated as less reliable than those from the Ga–O shell because no account of multiple scattering effects was taken during the data analysis. These effects may become increasingly significant beyond nearest-neighbour distances¹⁸ but cannot accurately be modelled in the case of an amorphous material.

X-ray absorption near-edge spectroscopy, XANES, spectra can also give information on the coordination environment of a given probe atom, often by comparison of the spectra with those from materials containing the probe atom in a well-defined structural site. In this case, we collected data with higher energy resolution in the vicinity Ga K-edge from reference materials, shown in Fig. 5 (a), and the glass samples containing 1, 3 and 5 mol% Ga₂O₃, shown in Fig. 5 (b). The reference materials were chosen to have a range of gallium coordination environments: quartz α -GaPO₄ contains tetrahedrally coordinated gallium¹⁶, β -Ga₂O₃ an equal mixture of tetrahedral and octahedral gallium²², and Ga(acac)₃ octahedral gallium²². Fig. 5 (a) shows that for the octahedrally-coordinated gallium a broad feature at ~10377 eV is observed, whilst for the tetrahedrally-coordinated gallium a distinct two-humped curve is seen in the same region with features centred at slightly higher and lower energy. The XANES spectrum from β -Ga₂O₃, the mixed-site material, contains features as observed in both the single-site materials. These qualitative observations are in agreement with previous studies which demonstrated

that different coordination sites could be distinguished using Ga K-edge XANES^{17,22,23}. The XANES spectra from the gallium-doped PBGs exhibit no variation as a function of composition and are similar to that measured from Ga(acac)₃.

IV. DISCUSSION

A. Cation coordination

Gallium ions in phosphate-based materials display an extraordinarily rich chemistry, adopting octahedral, tetrahedral and trigonal bipyramidal coordination. Of the crystalline anhydrous gallium phosphates, GaPO₄ has gallium in a tetrahedral environment¹⁶, Ga(PO₃)₃ contains octahedral gallium²⁴ and (NH₄)₃Ga₂(PO₄)₃²⁵ trigonal bipyramidal gallium. The diversity of gallium chemistry is further illustrated by the open framework structure of Na₃Ga₄O(OH)(H₂O)(PO₄)₄·H₂O which contains all three coordination geometries of gallium²⁶. The situation is similar in the amorphous state. HEXRD has previously been used to demonstrate that the coordination geometry of gallium varies as a function of composition in Ga₂O₃-P₂O₅ glasses with mostly tetrahedral gallium present at the pyrophosphate composition (Ga₄(P₂O₇)₃) and solely octahedral gallium present at the metaphosphate composition (Ga(PO₃)₃)²⁷. Ga K-edge EXAFS and ⁷¹Ga MAS NMR have also been used to identify octahedral, tetrahedral and trigonal bipyramidal coordinated gallium in Na₂O-Ga₂O₃-P₂O₅ glasses²⁸.

The XANES spectra presented here from the gallium-doped PBGs exhibit no variation as a function of composition and show one broad feature that is similar in

shape, intensity and magnitude to that observed for $\text{Ga}(\text{acac})_3$, suggesting that the Ga^{3+} ions in all the glass samples are octahedrally coordinated. Further evidence for octahedral coordination is provided by the EXAFS spectra and HEXRD data. Firstly, the EXAFS-derived Ga–O coordination numbers for the 3 and 5 mol% Ga_2O_3 samples are 6, within experimental error. Secondly, and more importantly, the measured Ga–O and Ga···P distances of 1.93 and 3.19 Å, respectively, show excellent agreement with those expected for octahedral gallium in a phosphate-based material. Ga–O distances show a strong correlation with coordination number: typical Ga–O distances for tetrahedral gallium fall in the range 1.82–1.84 Å, those for five coordinate gallium in the range 1.88–1.92 Å and those for octahedral gallium 1.94–1.99 Å²⁹. Furthermore, in phosphate-based materials, since the next nearest-neighbour atom is phosphorus which is part of the same anion as the nearest-neighbour oxygen atoms, one might expect a weaker correlation between metal coordination number and metal-phosphorus distance. In crystalline $\text{Ga}(\text{PO}_3)_3$, which contains octahedral gallium, the Ga–O and Ga···P distances are 1.95 and 3.24 Å, respectively²⁴, whereas the Ga–O and Ga···P distances for tetrahedral gallium in GaPO_4 are 1.85 and 3.07 Å, respectively¹⁶. Similar distances are observed in the amorphous state. Hoppe *et al.*²⁷ found average Ga–O and Ga···P distances of 1.93 and 3.20 Å, respectively, for octahedral gallium in $\text{Ga}(\text{PO}_3)_3$ glass and distances of 1.87 and 3.05 Å, respectively, in $\text{Ga}_4(\text{P}_2\text{O}_7)_3$. The latter material exhibited a Ga–O coordination number of 4.6, suggesting that it contained mostly tetrahedral gallium as suggested by the shortening of the average Ga–O and Ga···P distances. The Ga–O and Ga···P distances measured here show very close agreement with those of Hoppe measured for gallium in an octahedral environment in a phosphate-based glass. However, the Ga–O coordination numbers determined here from the HEXRD data are closer to 4 than 6. This

discrepancy can be explained by considering further the results of Hoppe. In that study, an asymmetric Ga–O peak, which had a tail extending to the high- r side of the mean position of ~ 1.9 Å, was observed for both compositions. Hoppe was able to simulate this peak shape with two Ga–O correlations because the high- r tail was well-resolved from the main O···O peak at ~ 2.5 Å. In our case, the situation is complicated by the presence of Na–O and Ca–O correlations at ~ 2.35 Å which render an accurate simulation of any high- r tail of the Ga–O peak impossible. Hence, the Ga–O coordination numbers measured here using HEXRD suggest that there is significant structural disorder around the gallium site which leads to a high- r contribution to the Ga–O peak which can not be accurately modelled in this data. This explanation is supported by the high EXAFS Debye-Waller factors for the Ga–O correlation which also suggest disorder in the GaO₆ octahedra.

The structural parameters derived from the HEXRD data also give information on the coordination of the Na⁺ and Ca²⁺ cations. The relevant parameters, shown in Table I, are typical of those determined by diffraction methods for PBGs containing Na⁺ and Ca²⁺ ions, with Na–O and Ca–O nearest-neighbour distances of close to 2.34 and 2.38 Å, respectively, and coordination numbers of ~ 4 for both correlations^{19,30}. The important result here is that no variation in the coordination of the Na⁺ and Ca²⁺ cations as a function of gallium content is observed.

B. Phosphate network

Phosphate glasses are often characterised in terms of the connectivity of the PO₄³⁻ tetrahedra that comprise the back-bone of their structures¹⁹. Predictions can be made concerning the phosphate connectivity on the basis of the glass composition,

specifically the O/P ratio¹⁹. The glasses studied here have O/P ratios in the range $3 < \text{O/P} < 3.5$, where the upper and lower limits in this range are the O/P ratios for the pyrophosphate ($\text{P}_2\text{O}_7^{4-}$) and metaphosphate (PO_3^-) compositions, respectively. Since metaphosphate glasses have structures consisting of rings and infinite chains of PO_4^{3-} tetrahedra and pyrophosphate glasses contain $\text{P}_2\text{O}_7^{4-}$ dimers, the glasses studied here are expected to contain rings and shorter, phosphate chains with the presence of only two types of phosphate species, *i.e.* $-\text{PO}_2^-$ middle groups and $-\text{PO}_3^{2-}$ chain-terminating end groups.

The structural parameters derived from the HEXRD data given in Table I describe both the individual PO_4^{3-} tetrahedra and their connectivity. Two P–O bond distances are used in the simulation of the PDF data, one at 1.60-1.61 Å ascribed to bonds to oxygen atoms that are shared between connected PO_4^{3-} tetrahedra (*i.e.* bridging oxygens, BOs) and one at 1.49 Å ascribed to bonds to non-bridging oxygen atoms (NBOs). For all three samples, a P–O coordination number of ~ 4 is observed as expected for structures based on PO_4^{3-} tetrahedra. No significant variation in the numbers of P–NBO and P–BO bonds is seen between samples, however, despite the variation in O/P ratio as a function of composition, *i.e.* 3.11, 3.18 and 3.22 for the 0, 3 and 5 mol% Ga_2O_3 samples, respectively, which should coincide with a change in connectivity within the phosphate network. This is most probably due to the difficulty in accurately modelling the two overlapping P–NBO and P–BO correlations, which highlights the limitations of the method.

The P...P coordination numbers in Table I can be compared to the expected values calculated on the basis of composition. The expected P...P coordination numbers for the 0, 3 and 5 mol% Ga_2O_3 samples are 1.8, 1.6 and 1.6, respectively, which are in reasonable agreement with the experimental values of 1.8, 1.7 and 1.7 in

Table I. Unfortunately, the errors of ± 0.3 associated with the experimental coordination numbers are larger than the expected decrease of 0.2 as a function of gallium content which means that we are limited in whether the experimentally observed decrease is significant. To help visualize the structural significance of the P...P coordination numbers, N_{PP} , we can calculate the average phosphate chain lengths, L , assuming that the structures are based entirely of linear chains composed of only $-\text{PO}_2^-$ middle groups and $-\text{PO}_3^{2-}$ end groups with an absence of rings:

$$L = \frac{2}{2 - N_{PP}} \quad (7)$$

Using the P...P coordination numbers calculated from the glass compositions, we arrive at average phosphate chain lengths of ~ 9 , ~ 6 and ~ 5 for the 0, 3 and 5 mol% Ga_2O_3 samples, respectively. This result shows that substituting only 5 mol% of the Na_2O with Ga_2O_3 in $(\text{P}_2\text{O}_5)_{0.45}(\text{CaO})_{0.16}(\text{Na}_2\text{O})_{0.39}$ glass can have a radical effect on its network structure.

To understand further the structural effects of adding Ga_2O_3 to a $(\text{P}_2\text{O}_5)_{0.45}(\text{CaO})_{0.16}(\text{Na}_2\text{O})_{0.39}$ glass, it is important to consider the role of the NBO atoms. In phosphate-based glasses between the pyrophosphate and metaphosphate compositions, the chains of PO_4^{3-} tetrahedra are usually linked by bonding interactions between the cations and the NBOs of the phosphate chains. In regard to this cross-linking of the phosphate chains, it is useful to consider the number of NBOs available to coordinate the cations. The number of NBOs per cation, N_{Me} , can easily be calculated from the glass composition³¹. For the glasses containing 0, 3 and 5 mol% Ga_2O_3 , there are 2.13, 2.26 and 2.34 N_{Me} , respectively. Since the experimental

results presented here exhibit no variation in Na–O and Ca–O coordination numbers as a function of glass composition, the N_{Me} values indicate that substitution of Na₂O with Ga₂O₃ results in more NBOs available to coordinate the gallium ions, resulting in the formation of GaO₆ octahedra. These GaO₆ octahedra block the migration of the remaining Na⁺ ions and increase the stability of the glass. A similar effect has been observed in phosphate glasses containing a few mol% of Fe₂O₃, where FeO₆ octahedra hinder the migration of other cations³².

The effect described, combined with the good glass-forming ability of gallium^{27,33} and the covalent nature of Ga–O–P bonding relative to Na–O–P bonding³³, provide a structural basis for the observed increase in chemical durability of Na₂O–CaO–P₂O₅ glasses when Ga₂O₃ replaces Na₂O¹². This is of direct relevance to the use of Na₂O–CaO–P₂O₅ glasses as controlled-delivery media for antimicrobial Ga³⁺ ions in biomedical applications. The results suggest that the concentration of Ga₂O₃ will be important, not only in terms of the total number of Ga³⁺ ions available for release, but also in terms of the overall stability and degradation rate of the glass matrix and therefore the rate with which those ions are released into body fluids.

V. CONCLUSION

The results of our structural study of antimicrobial gallium-doped phosphate-based glasses of general composition (P₂O₅)_{0.45}(CaO)_{0.16}(Na₂O)_{0.39-x}(Ga₂O₃)_x (where $x = 0.01, 0.03$ and 0.05) show that the Ga³⁺ ions occupy octahedral sites with respect to oxygen in all samples. Comparison of the HEXRD data with that from the glass containing no gallium reveals that the Ga³⁺ ions enter the phosphate network and reduce the average phosphate chain length. Substitution of Na₂O with Ga₂O₃ in Na₂O-

CaO-P₂O₅ glasses also increases the stability of the structure via the formation of GaO₆ octahedra which block the migration of the Na⁺ ions. This result is of direct relevance to the use of Na₂O-CaO-P₂O₅ glasses as controlled delivery media for antimicrobial Ga³⁺ ions in biomedical applications, suggesting that the level of Ga₂O₃ doping will affect both the concentration of Ga³⁺ ions available for release, and the overall stability and rate of degradation.

Acknowledgements

The authors wish to acknowledge funding from the STFC (EP/C000714, EP/C000633 and GR/T21080). We thank Bob Bilsborrow and Mark Roberts of the STFC Daresbury Laboratory for their assistance in the use of stations 16.5 and 9.1, respectively.

References

Electronic address: dmp@kent.ac.uk

- ¹ S. Hughes, *Curr. Opin. Orthop.* **3**, 69–73 (1992).
- ² M. E. Rupp, J. S. Ulphani, P. D. Fey, K. Bartscht, and D. Mack, *Infect. Immun.* **67** (5), 2627 (1999).
- ³ S. R. Norrby, C. E. Nord, and R. Finch, *Lancet Infect. Dis.* **5** (2), 115 (2005).
- ⁴ Y. Kaneko, M. Thoendel, O. Olakanmi, B. E. Britigan, and P. K. Singh, *J. Clin. Invest.* **117** (4), 877 (2007).
- ⁵ C. R. Chitambar and J. Narasimhan, *Pathobiology* **59** (1), 3 (1991).
- ⁶ O. Olakanmi, B. E. Britigan, and L. S. Schlesinger, *Infect. Immun.* **68** (10), 5619 (2000).

- 7 G. H. Yan, G. J. Wang, and Y. C. Li, *Acta Pharmacol. Sin.* **12** (6), 530 (1991).
- 8 J. R. Harrington, R. J. Martens, N. D. Cohen, and L. R. Bernstein, *J. Vet. Pharmacol. Ther.* **29** (2), 121 (2006).
- 9 J. C. Knowles, *J. Mater. Chem.* **13** (10), 2395 (2003).
- 10 S. H. Cartmell, P. J. Doherty, N. P. Rhodes, J. A. Hunt, D. M. Healy, and T. Gilchrist, *J. Mater. Sci.: Mater. Med.* **9** (1), 1 (1998).
- 11 T. Gilchrist, D. M. Healy, and C. Drake, *Biomaterials* **12** (1), 76 (1991).
- 12 S. V. Valappil, D. Ready, E. A. Abou Neel, D. M. Pickup, W. Chrzanowski, L. A. O'Dell, R. J. Newport, M. E. Smith, M. Wilson, and J. C. Knowles, *Adv. Funct. Mater.* **18** (5), 732 (2008).
- 13 L. R. Bernstein, *Pharmacol. Rev.* **50** (4), 665 (1998).
- 14 J. M. Cole, E. R. H. van Eck, G. Mountjoy, R. Anderson, T. Brennan, G. Bushnell-Wye, R. J. Newport, and G. A. Saunders, *J. Phys.: Condens. Matter* **13** (18), 4105 (2001).
- 15 P. H. Gaskell, *Materials Science and Technology*. (VCH, Weinheim, 1991).
- 16 S. N. Achary, O. D. Jayakumar, A. K. Tyagi, and S. K. Kulshresththa, *J. Solid State Chem.* **176** (1), 37 (2003).
- 17 R. I. Walton and D. O'Hare, *J. Phys. Chem. Solids* **62** (8), 1469 (2001).
- 18 J. J. Rehr, R. C. Albers, and S. I. Zabinsky, *Phys. Rev. Lett.* **69** (23), 3397 (1992).
- 19 R. K. Brow, *J. Non-Cryst. Solids* **263** (1-4), 1 (2000).
- 20 D. M. Pickup, G. Mountjoy, M. A. Roberts, G. W. Wallidge, R. J. Newport, and M. E. Smith, *J. Phys.: Condens. Matter* **12** (15), 3521 (2000).
- 21 J. M. Deleon, J. J. Rehr, S. I. Zabinsky, and R. C. Albers, *Phys. Rev. B* **44** (9), 4146 (1991); J. J. Rehr and R. C. Albers, *Rev. Mod. Phys.* **72** (3), 621 (2000).

- 22 K. Nishi, K. Shimizu, M. Takamatsu, H. Yoshida, A. Satsuma, T. Tanaka, S.
Yoshida, and T. Hattori, *J. Phys. Chem. B* **102** (50), 10190 (1998).
- 23 P. Charton and P. Armand, *J. Non-Cryst. Solids* **333** (3), 307 (2004).
- 24 N. Anissimova and R. Glaum, *Z. Anorg. Allg. Chem.* **624** (12), 2029 (1998).
- 25 F. Bonhomme, S. G. Thoma, and T. M. Nenoff, *Microporous Mesoporous
Mater.* **53** (1-3), 87 (2002).
- 26 A. Guesdon, Y. Monnin, and B. Raveau, *J. Solid State Chem.* **172** (2), 237
(2003).
- 27 U. Hoppe, D. Ilieva, and J. Neuefeind, *Z. Naturforsch., A: Phys. Sci.* **57** (8),
709 (2002).
- 28 A. Belkebir, J. Rocha, A. P. Esculcas, P. Berthet, S. Poisson, B. Gilbert, Z.
Gabelica, G. Llabres, F. Wijzen, and A. Rulmont, *Spectrochim. Acta, Part A*
56 (3), 423 (2000).
- 29 D. A. Fletcher, R. F. McMeeking, and D. Parkin, *J. Chem. Inf. Comput. Sci.*
36 (4), 746 (1996).
- 30 D. M. Pickup, P. Guerry, R. M. Moss, J. C. Knowles, M. E. Smith, and R. J.
Newport, *J. Mater. Chem.* **17**, 4777–4784 (2007).
- 31 U. Hoppe, G. Walter, R. Kranold, and D. Stachel, *J. Non-Cryst. Solids* **263** (1-
4), 29 (2000).
- 32 M. M. El-Desoky, K. Tahoona, and M. Y. Hassaan, *Mater. Chem. Phys.* **69**,
180 (2001).
- 33 D. Ilieva, B. Jivov, G. Bogachev, C. Petkov, I. Penkov, and Y. Dimitriev, *J.*
Non-Cryst. Solids **283** (1-3), 195 (2001).

Tables

TABLE I: Structural parameters obtained from the simulation of the HEXRD data from the $(\text{P}_2\text{O}_5)_{0.45}(\text{CaO})_{0.16}(\text{Na}_2\text{O})_{0.39-x}(\text{Ga}_2\text{O}_3)_x$ glasses [a].

Sample	Correlation	R (Å)	N	σ (Å)
x = 0	P–NBO	1.49(1)	1.9(3)	0.02(1)
	P–BO	1.61(1)	2.0(3)	0.06(1)
	Na–O	2.33(2)	4.0(6)	0.11(2)
	Ca–O	2.39(2)	4.4(7)	0.11(2)
	O...O	2.52(2)	4.6(7)	0.08(1)
	Na...O	2.81(2)	1.8(5)	0.14(4)
	P...P	2.94(2)	1.8(2)	0.08(2)
	x = 0.03	P–NBO	1.49(1)	2.0(3)
P–BO		1.60(1)	2.0(3)	0.05(1)
Ga–O		1.94(1)	4.1(9)	0.14(4)
Na–O		2.34(2)	4.1(6)	0.12(2)
Ca–O		2.38(2)	4.3(7)	0.08(2)
O...O		2.52(2)	4.8(5)	0.08(2)
Na...O		2.78(2)	1.8(4)	0.14(3)
P...P		2.94(4)	1.7(3)	0.07(2)
x = 0.05	P–NBO	1.49(1)	2.1(3)	0.01(1)
	P–BO	1.60(1)	2.1(3)	0.05(1)
	Ga–O	1.94(1)	4.1(9)	0.15(3)
	Na–O	2.35(2)	4.1(6)	0.11(2)
	Ca–O	2.38(2)	4.3(8)	0.07(2)
	O...O	2.53(2)	5.2(6)	0.10(2)
	Na...O	2.78(2)	1.9(5)	0.13(3)
	P...P	2.94(3)	1.7(3)	0.07(3)

[a] R is the atomic separation, N is the coordination number and σ is the disorder parameter

TABLE II: Structural parameters obtained from the simulation of the EXAFS data from the $(\text{P}_2\text{O}_5)_{0.45}(\text{CaO})_{0.16}(\text{Na}_2\text{O})_{0.39-x}(\text{Ga}_2\text{O}_3)_x$ glasses [a].

Sample	Correlation	R (Å)	N	A (Å ²)
x = 0.03	Ga–O	1.92(2)	6.6(13)	0.018(5)
	Ga...P	3.17(2)	2.9(12)	0.010(4)
x = 0.05	Ga–O	1.93(2)	6.6(13)	0.018(5)
	Ga...P	3.19(2)	3.2(13)	0.015(6)

[a] R is the atomic separation, N is the coordination number and A is the Debye-Waller factor

Figure Captions

FIG. 1: HEXRD data from the $(\text{P}_2\text{O}_5)_{0.45}(\text{CaO})_{0.16}(\text{Na}_2\text{O})_{0.39-x}(\text{Ga}_2\text{O}_3)_x$ glasses. (a) Q -space interference functions from the $x = 0$ (lower curve) and $x = 0.05$ (upper curve) samples, and (b) the real-space pair-distribution functions obtained by Fourier transformation of the Q -space data (solid lines) together with the simulations (dashed curves). Note that in each frame the upper curves have been offset for illustrative purposes.

FIG. 2: Difference pair-distribution function showing atomic correlations involving gallium (obtained by taking the difference between the pair-distribution functions shown in Fig. 1).

FIG. 3: Approximate X-ray scattering weighting factors for the difference pair-distribution function shown in Fig. 2.

FIG. 4: Ga K-edge EXAFS spectra from the $(\text{P}_2\text{O}_5)_{0.45}(\text{CaO})_{0.16}(\text{Na}_2\text{O})_{0.39-x}(\text{Ga}_2\text{O}_3)_x$ glasses. (a) k^3 weighted EXAFS (solid lines) with theoretical fits (dashed lines) from the $x = 0.03$ (lower curves) and $x = 0.05$ (upper curves) samples, and (b) Fourier transforms of these EXAFS spectra (solid lines) with theoretical fits (dashed lines). Note that in each frame the upper curves have been offset to aid clarity.

FIG. 5: Ga K-edge XANES spectra from (a) crystalline reference materials: quartz α - GaPO_4 (solid line), $\text{Ga}(\text{acac})_3$ (dashed line) and β - Ga_2O_3 (dotted line), and (b) $(\text{P}_2\text{O}_5)_{0.45}(\text{CaO})_{0.16}(\text{Na}_2\text{O})_{0.39-x}(\text{Ga}_2\text{O}_3)_x$ glasses: $x = 0.01$ (solid line), 0.03 (dashed line) and 0.05 (dotted line).

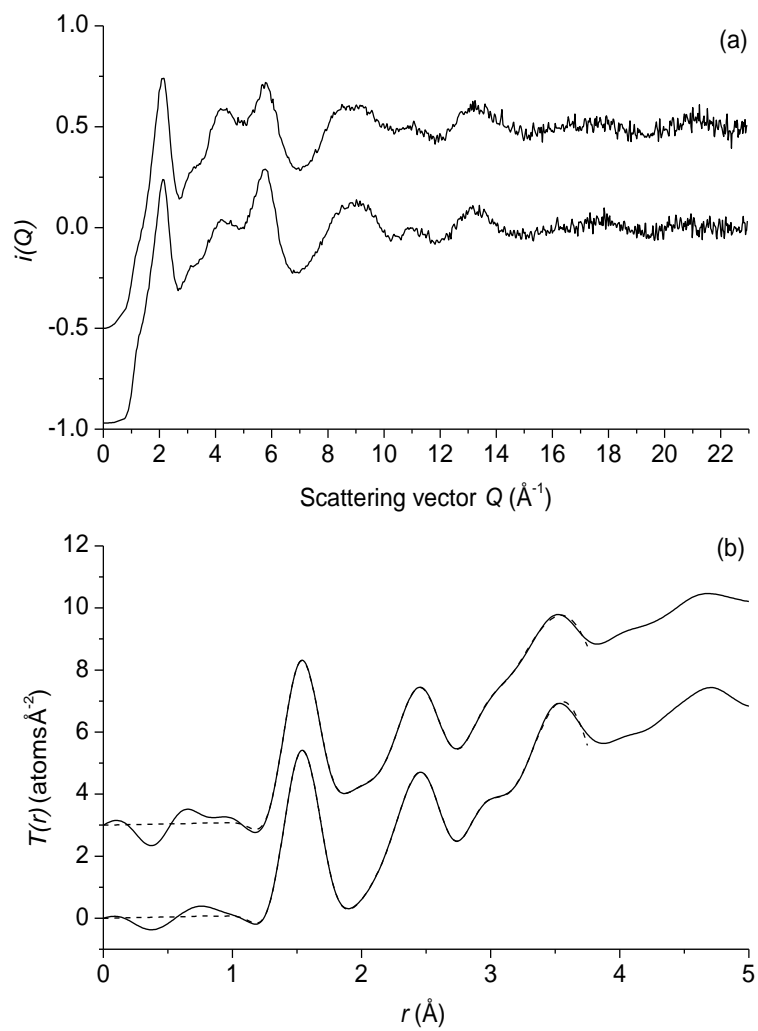
Figures**FIG1:**

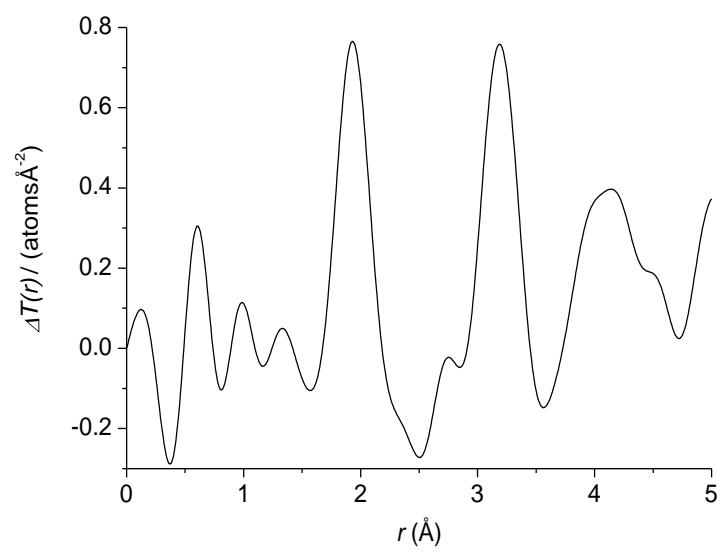
FIG. 2:

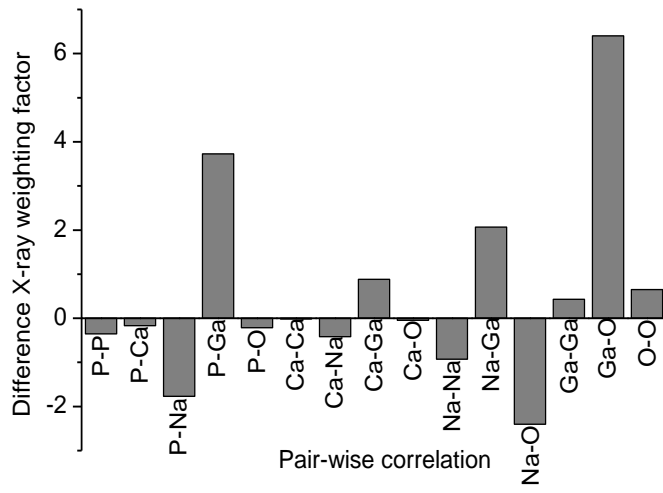
FIG 3:

FIG 4:

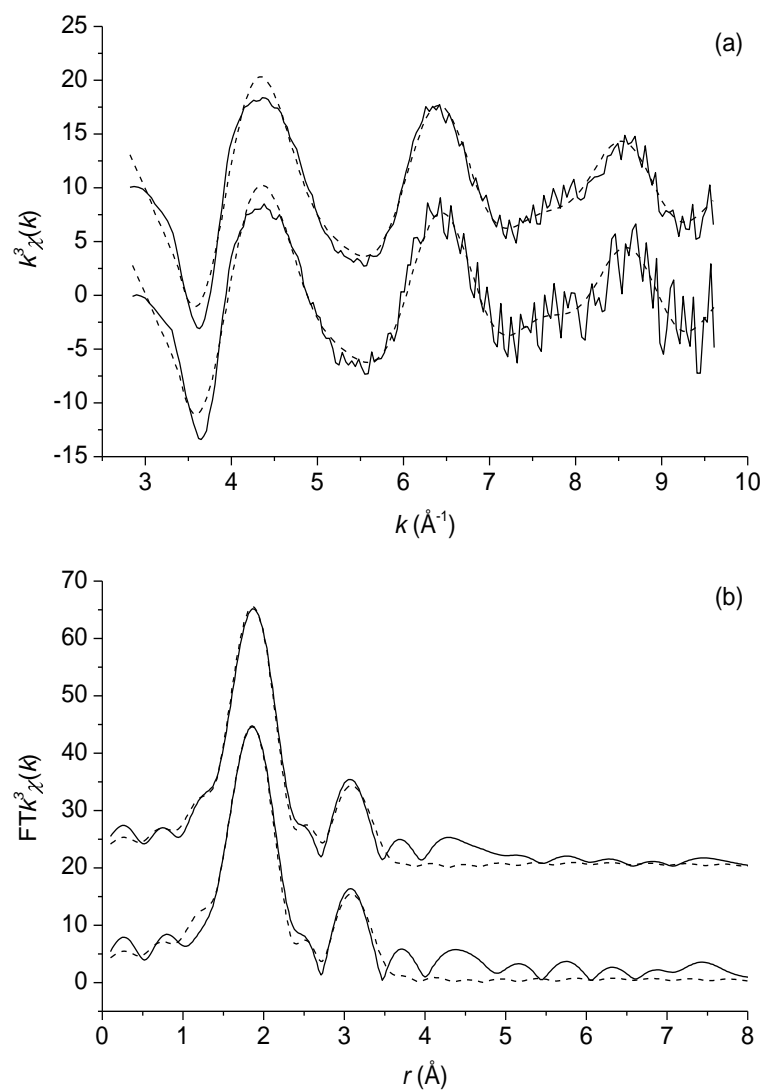


FIG. 5: